AD-A046 599 WASHINGTON UNIV SEATTLE DEPT OF MECHANICAL ENGINEERING F/G 13/13
A NUMERICAL DYNAMIC FRACTURE ANALYSES OF THREE WEDGE-LOADED DCB--ETC(U)
OCT 77 A S KOBAYASHI, S MALL, Y URABE N00014-76-C-0060

UNCLASSIFIED TR-29 NL

1 OF 1
AD A046599

END
DATE
FILMED
12-77
DDC

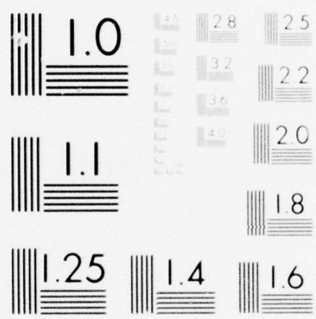
1.0
2.8
2.5
3.2
2.2
3.6
4.0
2.0
1.1
1.8
1.25
1.4
1.6

(12)

B.5

Office of Naval Research

Contract N00014-76-C-0060, NR 064-478

Technical Report No. 29

AD A 0 4 6 5 9 9

A NUMERICAL DYNAMIC FRACTURE ANALYSES OF THREE WEDGE-LOADED DCB SPECIMENS

By

A. S. Kobayashi, S. Mall, Y. Urabe and A. F. Emergy

October 1977

The research reported in this technical report was made possible through support extended to the Department of Mechanical Engineering, University of Washington, by the Office of Naval Research under Contract N00014-76-C-0060, NR 064-478. Reproduction in whole or in part is permitted for any purpose of the United States Government.

Department of Mechanical Engineering
College of Engineering
University of Washington

A NUMERICAL DYNAMIC FRACTURE ANALYSIS OF THREE WEDGE-LOADED DCB SPECIMENS

by

A. S. Kobayashi*, S. Mall**, Y. Urabe*** and A. F. Emery*

SUMMARY

A dynamic finite element code is used to compute the dynamic fracture toughness and crack arrest stress intensity factor from experimentally determined crack velocities in three fracturing wedge-loaded double cantilever beam (DCB) specimens. One experiment involving an Aradite-B DCB specimen by Kalthoff, et al., and two experiments involving Homalite-100 DCB specimens by Kobayashi, et al. and Irwin, et al. were analyzed by this hybrid numerical and experimental technique. Despite minor discrepancies, the computed dynamic fracture toughness and crack arrest stress intensity factors were in reasonable agreement with those determined experimentally. This comparative study between different experimental setups also indicates that the apparent differences in fracture dynamic responses could be attributed mainly to the differences in material properties, bluntness of the initial crack and specimen sizes and not to the differences in experimental techniques used.

INTRODUCTION

Over the past several years, Hahn et al. [1,2,3] have been developing wedge-loaded single/duplex double cantilever beam (DCB) specimens for determining the relation between dynamic fracture toughness, K_{ID}, and crack velocity and for measuring a crack arrest stress intensity factor, K_{Ia}. This specimen development was accompanied by Kanninen et al.'s comprehensive one and two-dimensional dynamic elastic analyses of the wedge-loaded DCB specimen [4,5] with fixed grip loading condition. Later analytical developments by Kanninen, et al. included the addition of a test machine compliance in the loading train for studying the effects of machine compliance on the dynamic response of a fracturing DCB specimen [6]. The dynamic responses of wedge-loaded DCB specimens have also been studied experimentally by dynamic photoelasticity [7,8] and the method of dynamic caustics [9]. It is not surprising that the three series of experiments resulted in somewhat different conclusions regarding the dynamic responses of these DCB specimens. The results of Reference [7], for example, casts doubts on the existence of a unique relation between dynamic fracture toughness and crack velocity and hence of a crack arrest stress intensity factor in the Homalite-100 plates used for fracture testing. On the other hand, a unique relation between dynamic fracture toughness and crack velocity is shown in Reference [8] for the same Homalite-100 material of larger thickness. The crack arrest stress intensity factor, K_{Ia}, was also found to be 95 percent of the static fracture toughness, K_{Ic}. Post arrest stress intensity factor was also observed to be slightly lower than K_{I_a} in agreement with the concept of K_{Ia} based on a static analysis sometime after crack arrest [10]. Recent fracture testings of Aradite-B specimens tend to confirm the above results where the crack arrest stress intensity factor, K_{Ia}, was found to be about equal to the fracture toughness. In these experiments, the dynamic stress intensity factors after crack arrest oscillated about the corresponding static value which varied with the crack velocity history [9] in apparent disagreement with findings of Reference [9].

* Professor, University of Washington, Department of Mechanical Engineering, Seattle, Washington 98195, USA.

** Postdoctoral Research Associate, University of Washington, Department of Mechanical Engineering, Seattle, Washington 98195, USA.

*** Postdoctoral Research Associate, University of Washington, Department of Mechanical Engineering, Seattle, Washington 98195, USA, currently on leave of absence from Mitsubishi Heavy Industries, Takasago Technical Institute, Takasago, Japan.

Inherent in the above widely varing conclusions of each series of experiments was the supposition that each result would be generally applicable to any other two dimensional dynamic fracture problems regardless of sizes, compliances of the loading systems and static and dynamic material properties thus each precluding the existence of the other two seemingly contradictory conclusions. Before assessing the possible variability in dynamic responses due to these test parameters, a standard DCB specimen of common geometry and loading system would have to be analyzed by the three groups of experimentalists in order to first assess the experimental accuracies of the techniques used. An alternate procedure would be to analyze the three different wedge-loaded DCB specimens with a common and reliable analytical technique. The agreement or disagreement between the analytical and experimental results could then provide some insight into the effects of specimen size and material properties on the dynamic responses of three different DCB specimens considered in References [7,8 and 9].

The objective of this paper is to use such analytical procedure for a comparative study of the dynamic responses of one typical fracture test results in each of References [7,8 and 9] for the purpose of deducing the effects of specimen geometries and material properties in these three separate test procedures.

DYNAMIC FINITE ELEMENT ANALYSIS

The procedure used is a two-dimensional, dynamic finite element code, HONDO [11], which was updated and modified for fracture dynamic analysis.* The basic modifications consisted of algorithms for startup and for computing dynamic stress intensity factor, dynamic energy release rate, fracture energy, kinetic energy and strain energy at each increment of crack advance.

In the startup procedure, the initial static stress distribution in a preloaded structure prior to dynamic crack propagation is computed. This initial stress distribution must be in complete static equilibrium prior to the initiation of a dynamic event. The finite element breakdown and hence the initial stiffness matrix used in this preliminary static analysis should be identical to those at the initiation or at the instant of time $t = 0+$ in the dynamic analysis. Close attention must be given to computational details. such as matching the 2x2 Gaussian integration points in the preliminary static and subsequent dynamic analyses in order to avoid any small differences between the finite element algorithms which will be sensed as unbalanced residual stresses and thus set off parasitic stress wave propagation in the HONDO II analysis.

In our past dynamic finite element analyses of fracturing Homalite-100 plates. considerable oscillations in the calculated dynamic energy release rates and hence in the dynamic stress intensity factors were noted [12.13]. Although the lack of such oscillations in the corresponding dynamic photoelasticity results are in part attributable to viscous damping in photoelastic polymers. much of the oscillations were thought to be generated through the instant release of crack-tip, finite element nodes during the process of discrete crack-tip advances. In order to reduce the impulse stress waves generated by such instantaneous release of a crack-tip node, the nodal force was reduced in equal increments which were determined by dividing the inter-nodal crack-tip transit time with the built-in finite time-increment in *HONDO II*. This procedure physically models a more gradual transit of the crack-tip between two adjacent finite element nodes. This nodal force release mechanism is similar to that developed by Keegstra [14-17] with the exception that the restraining nodal force is completely eliminated when the crack-tip reaches the adjacent node. The dissipated energy during such crack extension will be governed by the variations in nodal forces versus nodal displacement relation during crack extension. In general this nodal force versus nodal displacement relation is

* The updated finite element code is referred to as HONDO II.

non-linear and will be governed by the dynamic state surrounding the propagating crack tip thus requiring monitoring of nodal displacement at each incremental time if the dissipated energy is used for calculating dynamic energy release rates. The dynamic stress intensity factor can then be computed from the dynamic energy release rate using Freund's relation [17]. The generality of this relation in the presence of reflected stress waves in finite geometry was shown by Nilsson [18]. Alternatively, the near field dynamic stress field as derived by King et al. [19] can be used to calculate the dynamic stress intensity factor directly from the numerically obtained stresses either at the closest Gaussian integration point or at the center of a finite element which shares the crack tip node.

The appropriateness of the above procedures for computing a dynamic stress intensity factor was checked by analyzing the Broberg problem [20]. Figure 1 shows the coarse finite element breakdown used in analyzing a crack propagating at a high speed of $C/C_1 = 0.33$ where C and C_1 are the crack velocity and dilatational wave velocity in a steel, respectively. The large square finite element of 150 mm x 150 mm as well as the relatively high crack velocity used in this study simulated the extreme conditions experienced in another paper presented at this Symposium and thus served as an estimate of numerical errors involved in the latter [21].

Figure 2 shows the theoretical and computed crack opening displacements (COD) as the central crack starts to extend from zero crack length at constant rate. Despite the coarseness of the mesh, remarkable agreement between the computed and analytical CODs at even the first few increments of crack extension is noted. The coarseness of the finite element mesh at the initial phase of crack extension suggests that the near field COD equations from Reference [19] cannot be used effectively for computing the dynamic stress intensity factor, K_I^{dyn}. Since the adjacent Gaussian integration points and the center of the element was closer to the crack tip, an attempt was made to compute the dynamic stress intensity factor, K_I^{dyn} by using the near field, dynamic state of stresses as described in Reference [19]. The dynamic stress intensity factors computed from the normal and deviatoric stresses at the nearest Gaussian integration point, however, varied as much as 40 percent from the theoretical values and thus this procedure was abandoned. The dynamic stress intensity factor computed from the normal stress, σ_{yy}, at the center of the element as defined in Figure 3 were more stable and thus this K_I^{dyn} was compared against the theoretical solution as shown in Figure 3. Note that much of the spurious oscillations in the calculated dynamic stress intensity factors observed in previous analyses [12,13] were eliminated by the linearly increasing release of nodal force while the crack tip advanced from one finite element node to another. The initial large overestimation of K_I^{dyn}, as shown in Figure 3, could be attributed to the inappropriateness in using a one-term representation of the near field dynamic state of stress when the crack extended from zero crack length to 3 to 4 finite element lengths. However, remarkable agreements between computed and theoretical K_I^{dyn} are noted for longer crack length where the one-term representation of the near field dynamic state of stress becomes increasingly valid.

Although the above results indicate the need for finer element breakdown at the initial phase of the Broberg problem, such fine element breakdown for calculating K_I^{dyn} from the mid-element stress may not be always practical, since the time increment in dynamic finite element analysis is governed by the size of its smallest element. The strain energy release rate procedure of calculating static stress intensity factors from the results of finite element analysis, on the other hand, consistently provided accurate static stress intensity factors with relatively coarse meshes and thus the related dynamic energy release rate procedure was used to compute K_I^{dyn} for the same Broberg problem. As shown in Figure 3, notable improvement in the accuracy of K_I^{dyn} at the time of the first increment of crack propagation was made but the K_I^{dyn} after 3 to 4 incremental crack extensions was not as accurate as the K_I^{dyn} computed directly from the mid-element stress. Nevertheless, the proven accuracy of the energy release

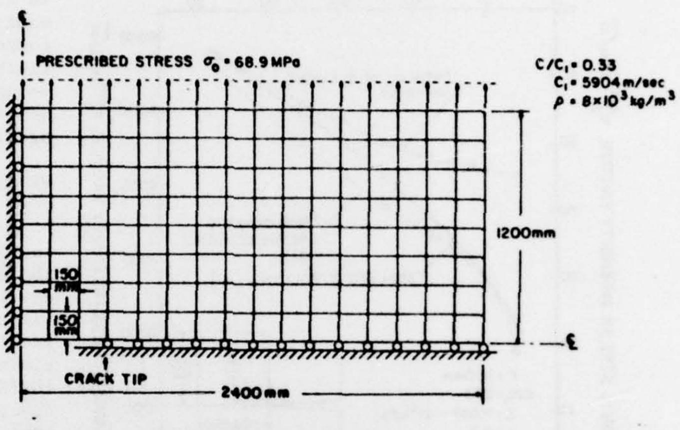

Figure 1. Finite Element Breakdown for Broberg's Problem.

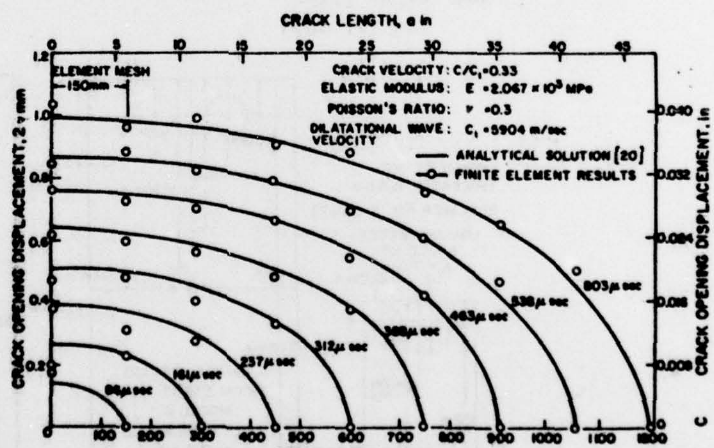

Figure 2. Computed Crack Opening Displacement of a Central Crack Expanding at a Constant Rate in a Uniaxial Stress Field of 68.9 MPa (10,000 psi).

rate procedure in static analysis and its reasonable accuracy in computing K_I^{dyn} with such coarse mesh of Figure 1, i.e. 150 mm square, at a high crack velocity of $C/C_1 = 0.33$ lead us to choose the procedure of dynamic energy release rate for computing K_I^{dyn} in our dynamic finite element analyses of the wedge-loaded DCB specimens as well as the crack arrest test specimens [21].

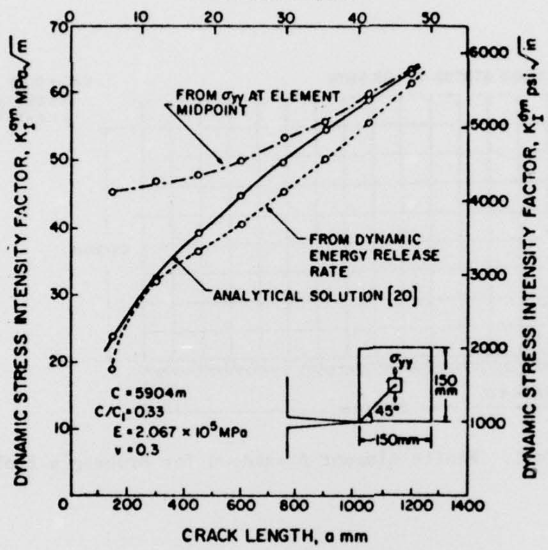

Figure 3. Dynamic Stress Intensity Factors of a Central Crack Expanding at a Constant Rate in a Uniaxial Stress Field of 68.9 MPa (10,000 psi).

WEDGE-LOADED DCB SPECIMENS

The three wedge-loaded DCB specimens which were analyzed by the dynamic finite element code described above are shown in Figure 4. For convenience in identification, the three specimens are designated as KML, IDKFE and KBW specimens, respectively. The static and dynamic material properties as determined by the three groups of investigators [7,8,9] are shown in Table 1. Although the static material properties were

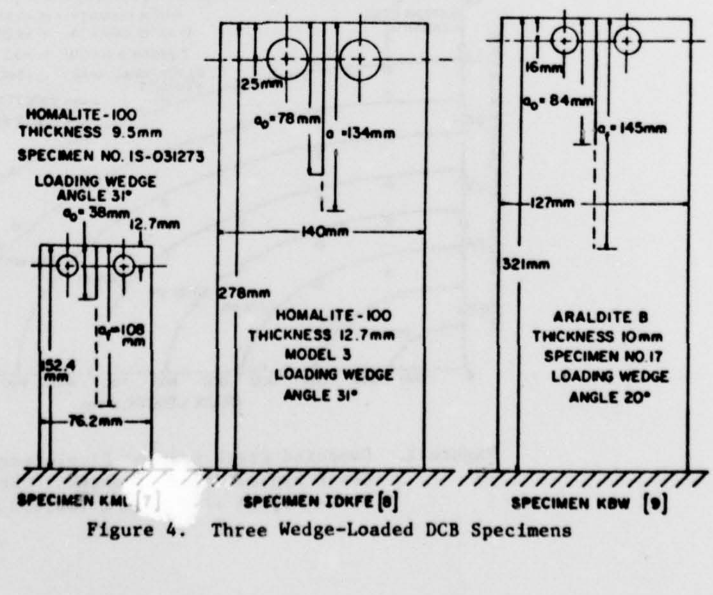

Figure 4. Three Wedge-Loaded DCB Specimens

Table 1 - Elastic Properties of Wedge-Loaded DCB Specimens

Specimen Identifica.	Material	Static		Dynamic	
		Modulus of Elasticity GP_a	Poisson's Ratio	Modulus of Elasticity GP_a	Poisson's Ratio
KML[7]	Homalite-100	3.72	0.345	4.65	0.345
IDKEF[8]	Homalite-100	3.89	0.31	4.82	0.31
KBW[9]	Araldite-B	3.38	0.33	3.66	0.39

comparable, the Araldite-B epoxy showed lesser strain sensitivity and higher static fracture toughness than the two Homalite-100 plates. The 30 to 40 percent differences in static and dynamic elastic moduli in the Homalite-100 plates forced the calculation to be conducted following the procedure [6] developed at Battelle's Columbus Laboratories. Basically, the procedure is to execute all static and dynamic analyses by using the static elastic modulus and then use the dynamic static modulus when computing the dynamic stress intensity factor from the dynamic energy release rate.* Identical fine meshes in the three finite element breakdowns, as shown in Figure 5, were used in analyzing all three specimens in order to minimize the numerical errors due to different fineness in finite element breakdown. The crack positions versus time relations for the three specimens, as shown in Figure 6, were then used to drive the crack at prescribed rates and the dynamic energy release rate, $\mathcal{G}_I^{dyn}$, and dynamic stress intensity factors, K_I^{dyn}, were computed following the procedure described above. It is interesting to note that the crack propagated comparable distances in all three specimens and that the crack velocity in the KML specimen was significantly higher than those in the IDKFE and KBW specimens.

RESULTS

KML Specimen [7]

A state of plane stress was assumed in the numerical analysis of this relatively thin Homalite-100 plate. The calculated and measured dynamic stress intensity factors as well as the calculated static stress intensity factor versus crack position are shown in Figure 7. Since the loading pin displacement at the onset of crack propagation was not measured in this series of experiments, the stress intensity factor for crack initiation, K_Q**, was estimated on the basis of matching the total dynamic energy released with the calculated total static strain energy released in this specimen. The resultant K_Q would thus be underestimated since no estimate of the extraneous dissipated energy in the specimen is included in this calculation. Reasonable agreement existed between the computed and measured K_D throughout the crack propagation except for the initial phase of crack propagation and in the region of momentary crack arrest. The isolated experimental point in the former was ignored in this comparison due to

* The superposition procedure developed in the original dynamic finite element analysis [12,13] handles this strain sensitivity problem by using static elastic modulus in the static calculation and dynamic elastic modulus in the dynamic analysis.

** Note that the subscript of I is dropped for all plane stress results.

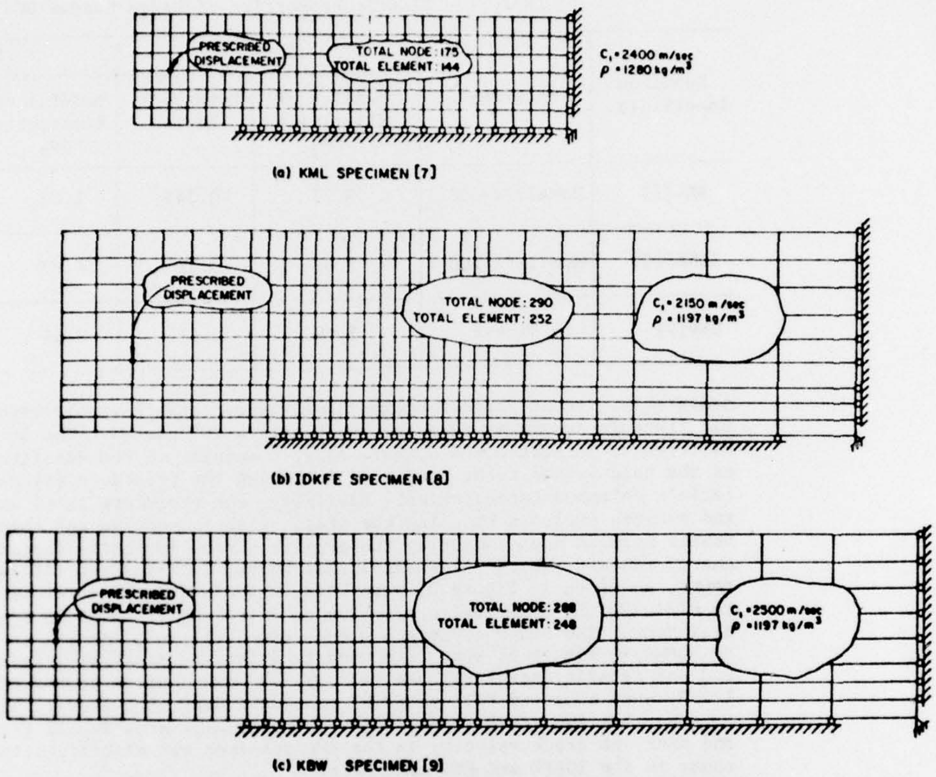

Figure 5. Finite Element Breakdowns of Three DCB Specimens

the blurriness in the dynamic isochromatic fringes and crack tip position which could have introduced large errors in K_D determination. The minor discrepancies between the experimental and calculated K_D in the region of crack arrest can be attributed to the dynamic finite element analysis which is sensitive to the variations in crack velocities. Crack velocities measurements in this region were not accurate due to the discrete recording of the crack which apparently arrested momentarily before starting up again.

IDKFE Specimen [8]

Figure 8 shows the variations in the calculated and measured dynamic stress intensity factors as well as the calculated static stress intensity factors. Note that the state of plane strain was assumed in the static and dynamic analyses of this specimen, not because this Homalite-100 specimen was thicker (13 mm versus 10 mm), but because the plane stress results yielded a lower K_D and increased the already existing discrepancies between measured and calculated results. Further study of the data in Table 2.14 and Figure 2.9 in Reference [8] indicated that perhaps the recorded wedge-pin-opening displacement in this experiment could be low thus providing a low K_{IQ} on which the entire static and dynamic calculations were based. If K_{IQ} was underestimated by say twenty percent, then the calculated static and dynamic stress intensity factor curves will shift upward and almost match the experimental dynamic stress intensity factors.

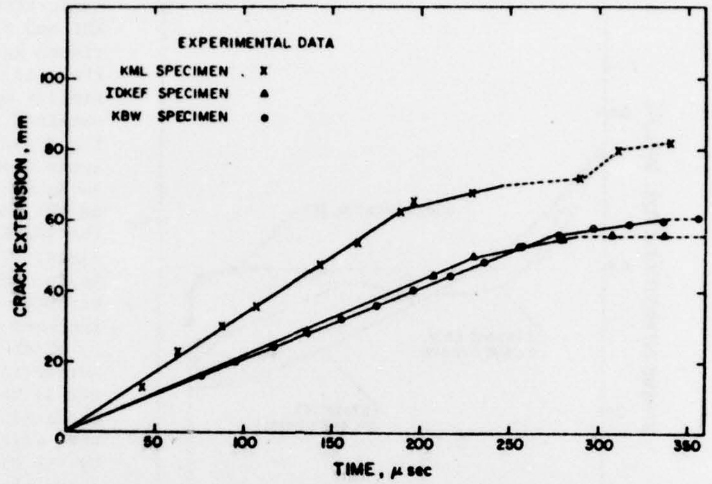

Figure 6. Crack Tip Position Versus Time in Wedge-Loaded DCB Specimens.

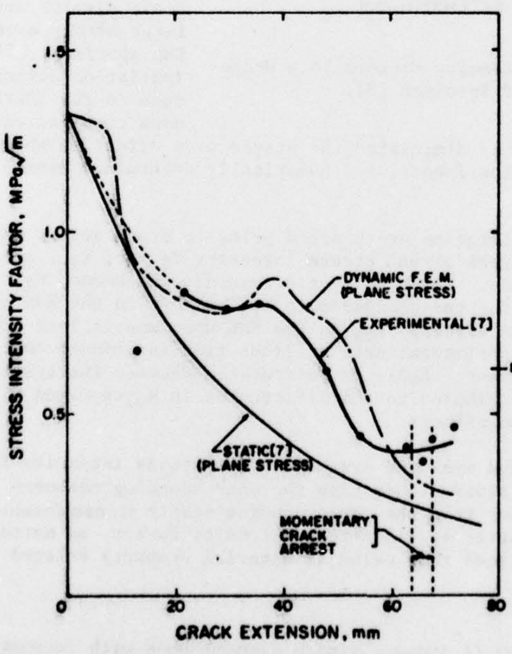

Figure 7. Stress Intensity Factors in a Wedge-Loaded DCB Specimen [7]

KWB Specimen [9]

Figure 9 shows the variations in the calculated and measured dynamic stress intensity factors as well as the calculated static stress intensity factors. Reasonable agreement in the calculated and measured K_D are seen, with minor differences in calculated and measured values in the region of crack arrest.

Figure 10 shows the calculated variations in energies with crack extension. These energy variations follow the characteristic rapid decrease in strain energy, an increase followed by a drop in kinetic energy and gradual increase in dissipated fracture energy [1-6]. The actual values differ with those in Figure 2.11 of Reference [6], particularly in the former two energies. Part of these discrepancies could be attributed to the one-dimensional analysis used in the Battelle code which would underestimate the strain energy and hence the fracture energy computed from energy balance.

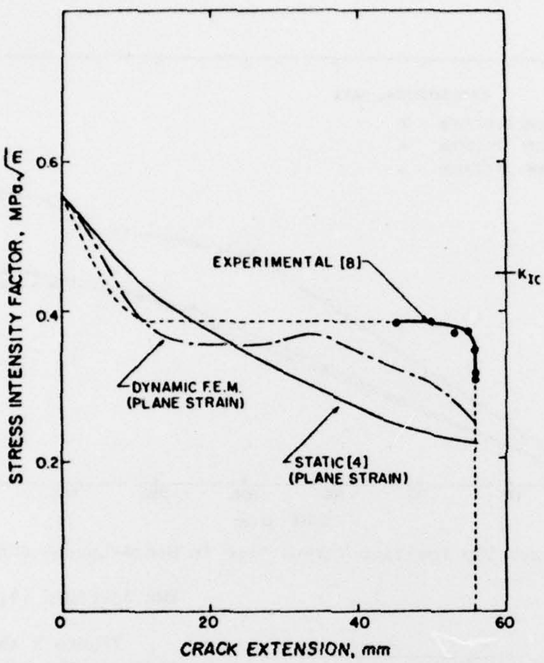

Figure 8. Stress Intensity Factors in a Wedge-Loaded DCB Specimen [8].

DISCUSSIONS

Calculated and measured dynamic stress intensity factors in KML and KBW wedge-loaded DCB specimens agreed reasonably well and there is reason to speculate that similar agreement would have been obtained in the IDKFE specimen. The dynamic finite element analysis reproduced the oscillations in K_D in the KML specimen as well as the relatively uniform K_{ID} in the IDKFE and K_D in the KBW specimen. The oscillations in K_D in the KML specimen could be attributed to the smallness in specimen size, as shown in Figure 4, which would generate higher interaction between the reflected stress waves and the propagating crack tip. This large stress wave effect was further augmented by the high K_Q value necessary to drive the crack approximately the same distance as in the other two IDKFE and KBW specimens. The computed overshoot in K_D immediately after crack propagation could also be attributed to the large stress wave effect in the KML specimen. The lower crack initiation stress intensity factors in the IDKFE and KBW specimens combined with the much longer specimen sizes obviously diminished the stress wave effect as shown by the lack of oscillations in the experimental and numerically determined dynamic stress intensity factors.

The gradual deceleration crack speed prior to crack arrest and thus the existence of a distinct crack arrest stress intensity factor, K_{Ia}, are noted in the IDKFE and KBW specimens. The high static fracture toughness, K_{Ic}, of Araldite-B could be responsible for the closeness in K_{Ia} and K_{Ic} in the KBW specimen as the crack slows down to an arrest. K_{Ia} in the KML specimen is less distinct, possibly due to the lack of experimental data at finer time increments during the period of momentary crack arrest. Again the difference between the crack arrest characteristics could be attributed to the differences in K_Q, specimen sizes and the associated stress wave effects.

The calculated and measured dynamic arrest stress intensity factors of the three specimens were always lower than the corresponding measured fracture toughnesses, K_{Ic}, and higher than the corresponding static stress intensity factor. The variability in the latter static stress intensity factor, as noted in Figures 7, 8 and 9, probably exclude this value as material property related to crack arrest.

CONCLUSIONS

The updated HONDO II dynamic finite element code with incremental release of crack tip nodal force has been shown to be a reliable procedure in analyzing fracture dynamic problems.

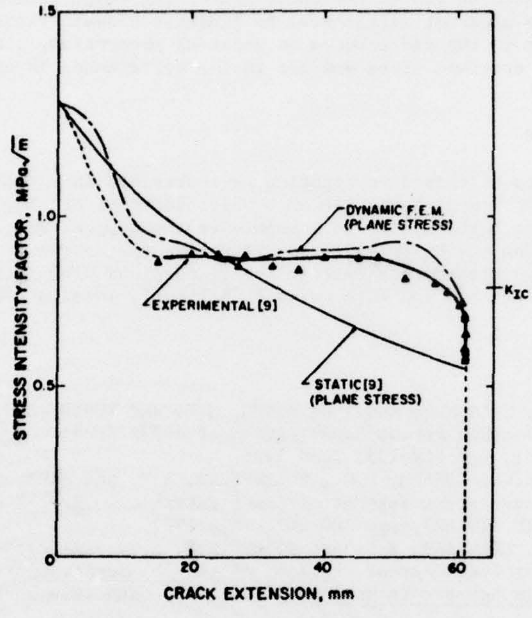

Figure 9. Stress Intensity Factors in a Wedge-Loaded DCB Specimen [9].

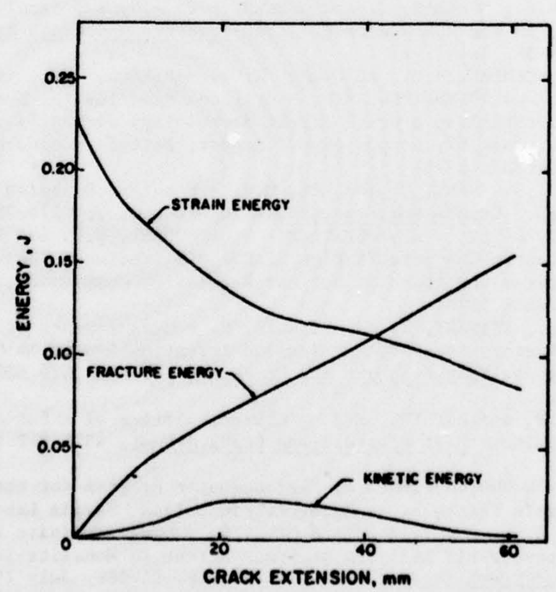

Figure 10. Energies in a Wedge-Loaded DCB Specimen [9].

This code successfully duplicated the experimentally determined dynamic fracture toughness in two of the three fracturing wedge-loaded DCB specimens and showed that the apparent differences in fracture dynamic responses could be attributed mainly to the differences in material properties, bluntness of the initial crack and specimen sizes and not to the differences in experimental techniques used.

ACKNOWLEDGEMENT

The results of this investigation were obtained in a research contract funded by the Office of Naval Research under Contract No. N00014-76-C-0060, NR 064-478. The authors wish to acknowledge the support and encouragement of Drs. N.R. Perrone and D. Mulville of ONR during the course of this investigation. The authors also wish to acknowledge the discussions with Professor W.L. Fourney, University of Maryland and with Dr. J.F. Kalthoff, Institut für Festkörpermechanik.

REFERENCES

1. HAHN, G.T., HOAGLAND, R.G., KANNINEN, M.F. and ROSENFIELD, A.R. - Pilot Study of Fracture Arrest Capabilities of A533B Steel. Cracks and Fracture, ASTM STP 601, pp. 209-233, June 1976.
2. HOAGLAND, R.G., GEHLEN, P.C., ROSENFIELD, A.F. and HAHN, G.T. - Characteristics of a Run-Arrest Segment of Crack Extension. Fast Fracture and Crack Arrest, ASTM STP 627, pp. 203-207, July 1977.
3. HAHN, G.T., HOAGLAND, R.G. and ROSENFIELD, A.R. - A Fracture Mechanics Practice for Crack Arrest. Trans. of the 4th Int'l. Conf. on Structural Mechanics in Reactor Technology, CECA, CEE, CEEA Luxembourg, Paper G 1/6, 1977.
4. KANNINEN, M.F. - A Dynamic Analysis of Unstable Crack Propagation and Arrest in the DCB Test Specimen. Int'l. J. of Fracture, Vol. 10, No. 3, pp. 415-431, September 1974.
5. KANNINEN, M.F., POPELAR, C. and GEHLEN, R.C. - Dynamic Analysis of Crack Propagation in the DCB Specimen. Fast Fracture and Crack Arrest, ASTM STP 627, pp. 19-38, July 1977.
6. HAHN, G.T., GEHLEN, R.C., HOAGLAND, R.G., MARSHALL, C.W., KANNINEN, M.F., POPELAR, C. and ROSENFIELD, A.F. - Critical Experiments, Measurements and Analyses to Establish a Crack Arrest Methodology for Nuclear Pressure Vessel Steels. Task 62, Second Annual Report, Battelle Columbus Laboratories BMI-1959, October 1976.
7. KOBAYASHI, A.S., MALL, S. and LEE, M.H. - Fracture Dynamics of Wedge-Loaded DCB Specimen. Cracks and Fracture, ASTM STP 601, pp. 274-290, June 1976.
8. IRWIN, G.R., DALLY, J.W., KOBAYASHI, T., FOURNEY, W.L. and ETHERIDGE, J.M. - A Photoelastic Characterization of Dynamic Fracture. University of Maryland Report prepared for the U.S. Nuclear Regulatory Commission, NUREG-0072, NRC-5, December 1976.
9. KALTHOFF, J., BEINERT, J. and WINKLER, S. - Measurements of Dynamic Stress Intensity Factors for Fast Running and Arresting Cracks in Double-Cantilever-Beam Specimens. Fast Fracture and Crack Arrest, ASTM STP 627, pp. 161-176, July, 1977.
10. CROSLEY, R.P. and RIPLING, E.J. - Characteristics of a Run-Arrest Segment of Crack Extension. Fast Fracture and Crack Arrest, ASTM STP 627, pp. 203-227, July 1977.
11. KEY, S.W. - HONDO, A Finite Element Computer Program for the Large Deformation Dynamic Responses of Axisymmetric Solids, Sandia Laboratories.
12. KOBAYASHI, A.S., EMERY, A.F. and MALL, S. - Dynamic Finite Element and Dynamic Photoelastic Analyses of Crack Arrest in Homalite-100 Plates, Fast Fracture and Crack Arrest, ASTM STP 627, pp. 95-108, July 1977.
13. KOBAYASHI, A.S., EMERY, A.F. and MALL, S. - Dynamic Finite Element and

Dynamic Photoelastic Analysis of Two Fracturing Homalite-100 Plates. Experimental Mechanics, Vol. 16, No. 9, pp. 321-328, September 1976.

14. KEEGSTRA, P.N.R. - A Transient Finite Element Crack Propagation Model for Nuclear Reactor Pressure Vessel Steels. J. Inst. Nucl. Engrs., Vol. 17, No. 4, pp. 89-96, 1976.
15. KEEGSTRA, P.N.R., HEAD, J.L. and TURNER, C.E. - A Transient Finite Element Analysis of Unstable Crack Propagation in Some 2-Dimensional Geometries. Proc. of the 4th Int'l. Conf. on Fracture, University of Waterloo Press, Vol. 3, pp. 515-522, 1977.
16. KEEGSTRA, P.N.R., HEAD, J.L. and TURNER, C.E. - The Interpretation of the Instrumented Charpy Test. Trans. of the 4th Int'l. Conf. on Structural Mechanics in Reactor Technology, Vol. G., CECA, CEE, CEEA Luxembourg, paper G 4/7, 1977.
17. FREUND, L.B. - Crack Propagation in an Elastic Solid Subjected to General Loading - II non-Uniform Rate of Extension. Journal of Mechanics and Physics of Solids, Vol. 20, 1972, pp. 141-152.
18. NILSSON, F. - A Note on the Stress Singularity at a Non-Uniformly Moving Crack Tip. Journal of Elasticity, Vol. 4, No. 1, March 1974, pp. 73-75.
19. KING, W.W., MALLUCK, J.F., ABERSON, J.A. and ANDERSON, J.M. - Application of Running Crack Eigenfunction to Finite Element Simulation of Crack Propagation. Mechanics Research Communication, Vol. 3, No. 3, pp. 197-202, 1976.
20. BORBERG, K.B. - The Propagation of a Brittle Crack. Arkiv fur Fysik, Vol. 18, pp. 159-198, 1960.
21. KANAZAWA, T., KOBAYASHI, A.S., MACHIDA, S. and URABE, Y. - Fracture Dynamic Analysis of Crack Arrest Test Specimens. To be published in the Proc. of this Symposium.

PART 1 - GOVERNMENT

Administrative and Liaison Activities

Office of Naval Research
Department of the Navy
Arlington, VA 22217
Attn: Code 474 (20
471
200

Director
Office of Naval Research Branch Office
495 Summer Street
Boston, MA 02210

Director
Office of Naval Research Branch Office
536 South Clark Street
Chicago, IL 60605

Director
Office of Naval Research
New York Area Office
715 Broadway - 5th Floor
New York, NY 10003

Director
Office of Naval Research Branch Office
1030 East Green Street
Pasadena, CA 91106

Director
Office of Naval Research
San Francisco Area Office
One Hallidie Plaza, Suite 601
San Francisco, CA 94102

Naval Research Laboratory (6)
Code 2627
Washington, D.C. 20375

Defense Documentation Center (12)
Cameron Station
Alexandria, VA 22314

NAVY

Naval Research Laboratory
Washington, D.C. 20375
Attn: Code 8400
8410
8430
8440
6300
6390
6380

Undersea Explosion Research Division
Naval Ship Research & Dev. Center
Norfolk Naval Shipyard
Portsmouth, VA 23709
Attn: Dr. E. Palmer, Code 177

Navy (Continued)

David W. Taylor Naval Ship Research
and Development Center
Annapolis, MD 21402
Attn: Code 2740
28
281

U.S. Naval Weapons Center
China Lake, CA 93555
Attn: Code 4062
4520

Commanding Officer
U.S. Naval Civil Engineering Laboratory
Code L31
Port Hueneme, CA 93041

Naval Surface Weapons Center
White Oak
Silver Spring, MD 20910
Attn: Code WR-10
WA-20

Technical Director
Naval Ocean Systems Center
San Diego, CA 92152

Supervisor of Shipbuilding
U.S. Navy
Newport News, VA 23607

U.S. Navy Underwater Sound Reference Division
Naval Research Laboratory
P.O. Box 8337
Orlando, FL 32806

Chief of Naval Operations
Department of the Navy
Washington, DC 20350
Attn: Code OP-098

Strategic Systems Project Office
Department of the Navy
Washington, DC 20376
Attn: NSP-200

Naval Air Systems Command
Department of the Navy
Washington, DC 20361
Attn: Code 5302 (Aerospace & Structures)
604 (Technical Library)
320B (Structures)

Naval Air Development Center
Director, Aerospace Mechanics
Warminster, PA 18974

U.S. Naval Academy
Engineering Department
Annapolis, MD 21402

NASA (Continued)

Scientific & Technical Information Facility
NASA Representative (S-AK/DL)
P.O. Box 5700
Bethesda, MD 20014

Other Government Activities

Commandant
Chief, Testing & Development Division
U.S. Coast Guard
1300 E Street, NW
Washington, DC 20226

Technical Director
Marine Corps Development and
Education Command
Quantico, VA 22134

Director
National Bureau of Standards
Washington, DC 20034
Attn: Mr. B.L. Wilson, EM 219

Dr. M. Gaus
National Science Foundation
Environmental Research Division
Washington, DC 20550

Library of Congress
Science and Technology Division
Washington, DC 20540

Director
Defense Nuclear Agency
Washington, DC 20305
Attn: SPSS

Director Defense Research & Engineering
Technical Library
Room 3C128
The Pentagon
Washington, DC 20301

Mr. Jerome Persh
Staff Specialist for Materials
and Structures
ODDR&E, The Pentagon
Room 3D1089
Washington, DC 20301

Chief, Airframe & Equipment Branch
FS-120
Office of Flight Standards
Federal Aviation Agency
Washington, DC 20553

Chief, Research and Development
Maritime Administration
Washington, DC 20235

Picatinny Arsenal
Plastics Technical Evaluation Center
Attn: Technical Information Center
Dover, NJ 07801

Other Government Activities (Continued)

Deputy Chief, Office of Ship Construction
Maritime Administration
Washington, DC 20235
Attn: Mr. U.L. Russo

National Academy of Sciences
National Research Council
Ship Hull Research Committee
2101 Constitution Avenue
Washington, DC 20418
Attn: Mr. A.R. Lytle

National Science Foundation
Engineering Mechanics Section
Division of Engineering
Washington, DC 20550

Commander Field Command
Defense Nuclear Agency
Sandia Base
Albuquerque, NM 87115

Atomic Energy Commission
Div. of Reactor Dev. & Tech.
Germantown, Maryland 20767

Navy (Continued)

Naval Facilities Engineering Command
200 Stovall Street
Alexandria, VA 22332
Attn: Code 03 (Research & Development)
048
045
14114 (Technical Library)

Naval Sea Systems Command
Department of the Navy
Washington, DC 20362
Attn: Code 03 (Research & Technology)
037 (Ship Silencing Division)
035 (Mechanics & Materials)

Naval Ship Engineering Center
Department of the Navy
Washington, DC 20362
Attn: Code 6105G
6114
6120D
6128
6129

Commanding Officer and Director
David W. Taylor Naval Ship Research
and Development Center
Bethesda, MD 20034
Attn: Code 042
17
172
173
174
1800
1102.1
1900
1901
1945
1960
1962

Naval Underwater Systems Center
Newport, RI 02840
Attn: Dr. R. Trainor

Naval Surface Weapons Center
Dahlgren Laboratory
Dahlgren, VA 22448
Attn: Code DG-20
DG-30

Technical Director
Mare Island Naval Shipyard
Vallejo, CA 94592

Army

Commanding Officer (2)
U.S. Army Research Office
P.O. Box 12211
Research Triangle Park, NC 27709
Attn: Mr. J.J. Murray, CRD-AA-IP

Army (Continued)

Watervliet Arsenal
MAGGS Research Center
Watervliet, NY 12189
Attn: Director of Research

U.S. Army Materials and Mechanics
Research Center
Watertown, MA 02172
Attn: Dr. R. Shea, DRXMR-T

U.S. Army Missile Research & Dev. Center
Redstone Scientific Information Center
Chief, Document Section
Redstone Arsenal, AL 35809

Army Research and Development Center
Fort Belvoir, VA 22060

Air Force

Commander WADD
Wright-Patterson Air Force Base
Dayton, OH 45433
Attn: Code WWRMDD
AFFDL (FDDS)
Structures Division
AFLC (MCEEA)

Chief, Applied Mechanics Group
U.S. Air Force Institute of Technology
Wright-Patterson Air Force Base
Dayton, OH 45433

Chief, Civil Engineering Branch
WLRC, Research Division
Air Force Weapons Laboratory
Kirtland Air Force Base
Albuquerque, NM 87117

Air Force Office of Scientific Research
Bolling Air Force Base
Washington, DC 20332
Attn: Mechanics Division

Department of the Air Force
Air University Library
Maxwell Air Force Base
Montgomery, AL 36112

NASA

National Aeronautics & Space Administration
Structures Research Division
Langley Research Center
Langley Station
Hampton, VA 23365

National Aeronautics & Space Administration
Associate Administrator for Advanced
Research and Technology
Washington, D.C 02546

PART 2 - CONTRACTORS AND OTHER TECHNICAL COLLABORATORS

Universities

Dr.J. Tinsley Oden
University of Texas at Austin
345 Engineering Science Building
Austin, TX 78712

Professor Julius Miklowitz
California Institute of Technology
Div. of Engineering & Applied Sciences
Pasadena, CA 91109

Dr. Harold Liebowitz, Dean
School of Engineering & Applied Science
George Washington University
Washington, DC 20052

Professor Eli Sternberg
California Institute of Technology
Div. of Engineering & Applied Science
Pasadena, CA 91109

Professor Paul M. Naghdi
University of California
Department of Mechanical Engineering
Berkeley, CA 94720

Professor P.S. Symonds
Brown University
Division of Engineering
Providence, RI 02912

Professor A.J. Durelli
Oakland University
School of Engineering
Rochester, MI 48063

Professor F.L. DiMaggio
Columbia University
Department of Civil Engineering
New York, NY 10027

Professor Norman Jones
Massachusetts Institute of Technology
Department of Ocean Engineering
Cambridge, MA 02139

Professor E.J. Skudrzyk
Pennsylvania State University
Applied Research Laboratory
Department of Physics
State College, PA 16801

Professor J. Kempner
Polytechnic Institute of New York
Dept. of Aerospace Engrg. & Applied Mech.
333 Jay Street
Brooklyn, NY 11201

Professor J. Klosner
Polytechnic Institute of New York
Dept. of Aerospace Engrg. & Applied Mechanics
333 Jay Street
Brooklyn, NY 11201

Professor R.A. Schapery
Texas A&M University
Department of Civil Engineering
College Station, TX 77843

Professor Walter D. Pilkey
University of Virginia
Research Laboratories for the Engineering
Sciences
School of Engineering and Applied Sciences
Charlottesville, VA 22901

Professor K.D. Willmert
Clarkson College of Technology
Department of Mechanical Engineering
Potsdam, NY 13676

Dr. H.G. Schaeffer
University of Maryland
Aerospace Engineering Department
College Park, MD 20742

Dr. Walter E. Haisler
Texas A&M University
Aerospace Engineering Department
College Station, TX 77843

Dr. B.S. Berger
University of Maryland
Department of Mechanical Engineering
College Park, MD 20742

Dr. L.A. Schmit
University of California
School of Engineering & Applied Science
Los Angeles, CA 90024

Dr. Hussein A. Kamel
University of Arizona
Dept. of Aerospace & Mechanical Engineering
Tucson, AZ 85721

Dr. S.J. Fenves
Carnegie-Mellon University
Department of Civil Engineering
Schenley Park
Pittsburgh, PA 15213

Dr. Ronald L. Huston
Dept. of Engineering Analysis
University of Cincinnati
Cincinnati, OH 45221

Universities (Continued)

Professor G.C.M. Sih
Lehigh University
Institute of Fracture and
Solid Mechanics
Bethlehem, PA 18015

Professor Albert S. Kobayashi
University of Washington
Department of Mechanical Engineering
Seattle, WA 98195

Professor Daniel Frederick
Virginia Polytechnic Institute and
State University
Dept. of Engineering Mechanics
Blacksburg, VA 24061

Professor A.C. Eringen
Dept. of Aerospace & Mech. Sciences
Princeton University
Princeton, NJ 08540

Professor E.H. Lee
Stanford University
Div. of Engineering Mechanics
Stanford, CA 94305

Professor Albert I. King
Wayne State University
Biomechanics Research Center
Detroit, MI 48202

Dr. V.R. Hodgson
Wayne State University
School of Medicine
Detroit, MI 48202

Dean B.A. Boley
Northwestern University
Department of Civil Engineering
Evanston, IL 60201

Professor P.G. Hodge, Jr.
University of Minnesota
Dept. of Aerospace Engineering
and Mechanics
Minneapolis, MN 55455

Dr. D.C. Drucker
University of Illinois
Dean of Engineering
Urbana, IL 61801

Professor N.M. Newmark
University of Illinois
Dept. of Civil Engineering
Urbana, IL 61803

Professor E. Reissner
University of California, San Diego
Dept. of Applied Mechanics
La Jolla, CA 92037

Professor William A. Nash
University of Massachusetts
Dept. of Mechanics & Aerospace Engineering
Amherst, MA 01002

Professor G. Herrmann
Stanford University
Department of Applied Mechanics
Stanford, CA 94305

Professor J.D. Achenbach
Northwestern University
Department of Civil Engineering
Evanston, IL 60201

Professor G.R. Irwin
University of Maryland
Dept. of Mechanical Engineering
College Park, MD 20742

Professor S.B. Dong
University of California
Department of Mechanics
Los Angeles, CA 90024

Professor Burt Paul
University of Pennsylvania
Towne School of Civil and
Mechanical Engineering
Philadelphia, PA 19104

Professor H.W. Liu
Syracuse University
Dept. of Chemical Engineering & Metallurgy
Syracuse, NY 13210

Professor S. Bodner
Technion R&D Foundation
Haifa, Israel

Professor Werner Goldsmith
University of California
Dept. of Mechanical Engineering
Berkeley, CA 94720

Professor R.S. Rivlin
Lehigh University
Center for the Application of Mathematics
Bethlehem, PA 18015

Professor F.A. Cozzarelli
State University of New York at Buffalo
Div. of Interdisciplinary Studies
Karr Parker Engineering Building
Chemistry Road
Buffalo, NY 14214

Professor Joseph L. Rose
Drexel University
Dept. of Mechanical Engineering & Mechanics
Philadelphia, PA 19104

Universities (Continued)

Professor Kent R. Wilson
University of California, San Diego
Department of Chemistry
La Jolla, CA 92093

Professor B.K. Donaldson
University of Maryland
Aerospace Engineering Department
College Park, MD 20742

Professor Joseph A. Clark
Catholic University of America
Dept. of Mechanical Engineering
Washington, DC 20064

Professor T.C. Huang
University of Wisconsin-Madison
Dept. of Engineering Mechanics
Madison, WI 53706

Dr. Samuel B. Batdorf
University of California
School of Engineering & Applied Science
Los Angeles, CA 90024

Industry and Research Institutes

U.S. Naval Postgraduate School
Library
Code 0384
Monterey, CA 93940

Webb Institute of Naval Architecture
Attn: Librarian
Crescent Beach Road, Glen Cove
Long Island, NY 11542

Unclassified

SECURITY CLASSIFICATION OF THIS PAGE (When Data Entered)

REPORT DOCUMENTATION PAGE

READ INSTRUCTIONS BEFORE COMPLETING FORM

1. REPORT NUMBER (14) TR ~~No~~ 29	2. GOVT ACCESSION NO.
3. RECIPIENT'S CATALOG NUMBER TR No. 29	
4. TITLE (and Subtitle) (6) A Numerical Dynamic Fracture Analyses of Three Wedge-Loaded DCB Specimens,	5. TYPE OF REPORT & PERIOD COVERED (9) Interim Report,
	6. PERFORMING ORG. REPORT NUMBER 29
7. AUTHOR(s) (10) A.S. Kobayashi, S. Mall, Y. Urabe and A.F. Emery	8. CONTRACT OR GRANT NUMBER(s) (15) N00014-76-C-0060, NR 064-478
9. PERFORMING ORGANIZATION NAME AND ADDRESS University of Washington, Department of Mechanical Engineering, Seattle, Washington 98195	10. PROGRAM ELEMENT, PROJECT, TASK AREA & WORK UNIT NUMBERS
11. CONTROLLING OFFICE NAME AND ADDRESS Office of Naval Research, Arlington, Virginia (12) 13p.	12. REPORT DATE (11) October 1977
	13. NUMBER OF PAGES 12
14. MONITORING AGENCY NAME & ADDRESS(if different from Controlling Office)	15. SECURITY CLASS. (of this report) unclassified
	15a. DECLASSIFICATION/DOWNGRADING SCHEDULE

16. DISTRIBUTION STATEMENT (of this Report)

unlimited

DISTRIBUTION STATEMENT A
Approved for public release;
Distribution Unlimited

17. DISTRIBUTION STATEMENT (of the abstract entered in Block 20, if different from Report)

18. SUPPLEMENTARY NOTES

19. KEY WORDS (Continue on reverse side if necessary and identify by block number)

Fracture Mechanics
Crack Propagation
Crack Arrest
Impact
Dynamic Photoelasticity

20. ABSTRACT (Continue on reverse side if necessary and identify by block number)

A dynamic finite element code is used to compute the dynamic fracture toughness and crack arrest stress intensity factor from experimentally determined crack velocities in three fracturing wedge-loaded double cantilever beam (DCB) specimens. One experiment involving an Aradite-B DCB specimen by Kalthoff, et al., and two experiments involving Homalite-100 DCB specimens by Kobayashi, et al. and Irwin, et al. were analyzed by this hybrid numerical and experimental technique. Despite minor discrepancies, the computed dynamic fracture toughness and crack
(continued on reverse) over

DD FORM 1 JAN 73 1473 EDITION OF 1 NOV 65 IS OBSOLETE
S/N 0102-014-6601

Unclassified

SECURITY CLASSIFICATION OF THIS PAGE (When Data Entered)

400 344 1B

20. (Continued)

arrest stress intensity factors were in reasonable agreement with those determined experimentally. This comparative study between different experimental setups also indicates that the apparent differences in fracture dynamic responses could be attributed mainly to the differences in material properties, bluntness of the initial crack and specimen sizes and not to the differences in experimental techniques used.